Design Optimization of Spoke-type Flux-intensifying PM Motor with Asymmetric Rotor Configuration for Improved Performance

Min-Fu Hsieh[1*], *Senior, IEEE,* Anh Thanh Huynh[2], *Member, IEEE,* Viet-Vu Do[1], David Gerada[2], *Senior, IEEE* and Chris Gerada[2], *Senior, IEEE*

[1]Department of Electrical Engineering, National Cheng Kung University, Tainan 701, Taiwan, mfhsieh@mail.ncku.edu.tw
[2]Power Electronics and Machines Centre, University of Nottingham, Nottingham, NG7 2GT, UK, anh.huynh@nottingham.ac.uk

This article explores enhancing spoke-type flux-intensifying permanent magnet (SFI-PM) motor performance by strategically placing flux barriers (FBs) in the asymmetric rotor. Integrating multi-flux barriers into the conventional spoke-type PM (CSPM) rotor topology elevates the d-axis inductance ($L_d > L_q$), intensifying flux density and improving output torque while posing challenges like increased cogging torque, torque ripple, and harmonic distortion. An asymmetric rotor design is proposed to mitigate these issues by strategically placing a higher number of flux barriers along the forward direction of the spoke magnet axis (q-axis). Analysis reveals that this configuration reduces torque ripple and enhances output torque. A Multi-Objective Genetic Algorithm (MOGA) is applied to optimize this asymmetric design considering mechanical constraints. The analyses are validated by manufacturing and testing a 5 kW asymmetric SFI-PM machine with a higher number of flux barriers along the forward direction of the spoke magnet axis.

***Index Terms*— flux-intensifying PM motor, spoke-type permanent magnet motor, asymmetric multi-flux barriers, flux-intensifying effect, demagnetization risks.**

I. Introduction

FLUX-intensifying (FI) permanent magnet (FI-PM) machines offer significant advantages over conventional permanent magnet synchronous machines (PMSMs), such as a lower risk of irreversible demagnetization, reduced magnet usage, higher output torque, and an improved constant power speed range (CPSR) [1-3]. These machines have gained attention due to their ability to use positive d-axis current (i_d) to intensify flux density, known as the FI effect. With greater d-axis inductance compared to q-axis inductance, FI-PM machines can apply FI current to gain both reluctance and electromagnetic torque.. This enhances motor performance, reduces demagnetization risks, and lowers initial costs by enabling the use of thinner magnets [3, 4].

Inserting multiple flux barriers (FBs) into PMSM rotors effectively creates the FI effect, but it also increases cogging torque, torque ripple, and harmonic distortion [3, 5, 6]. Minimizing these issues is crucial due to their impact on noise and vibration. Studies show that asymmetric rotor designs can mitigate these challenges and enhance motor performance [7-11]. Asymmetric rotor design can be categorized into two primary types: (1) incorporating one or more PM layers or flux barriers on the d- or q-axis of the rotor core [7-10] and (2) utilizing the magnet-axis-shifting effect [11, 12]. Typically, an asymmetric design with additional FBs is implemented in the forward direction (FD) of the spoke magnet axis (q-axis) or the d-axis of the V-shaped magnet type, aligned with the rotor core's rotational direction [7, 10]. Additionally, adding PM layers in the reverse direction (RD) of the d-axis with the V-shaped magnet type creates an asymmetric rotor [8, 9]. This method resembles the magnet-axis-shifting effect, where the magnet-axis (d-axis) of a V-shaped or Delta-shaped magnet is shifted to the RD [11, 12]. Clearly, there are no definitive guidelines for designing asymmetric rotors in PMSM machines to reduce cogging torque or torque ripples while enhancing overall performance.

In symmetric rotor designs, the flux density distribution is balanced along the d-axis. In contrast, asymmetric rotor designs have unbalanced flux distribution due to the placement of asymmetric components. While symmetric designs ensure consistent motor performance regardless of rotation direction, adding asymmetric components like additional PM layers, FBs, or magnet-axis shifting can significantly impact cogging torque, torque ripple, and output torque. Therefore, it is crucial to thoroughly investigate the placement to put asymmetric elements, such as FBs, within the rotor core. This is especially vital for multiple FB of an FI-PM motor, which aims to significantly enhance the FI effect while simultaneously reducing cogging torque and torque ripple.

In this study, flux barriers (FBs) are initially symmetrically positioned on the rotor in both the forward (FD) and reverse directions (RD) of the spoke magnet axis (q-axis) within a conventional spoke-type PM (CSPM) motor. This setup aims to enhance flux intensity and motor performance but increases cogging torque, torque ripple, and harmonic distortion. To address these challenges, this paper explores the impact of creating asymmetric rotor designs by strategically placing FBs. Specifically, two positions beside the q-axis in the rotor core are considered for FB placement to enhance the FI effect while reducing cogging torque and torque ripple. The performance of these asymmetric designs will be analyzed and compared with symmetrical rotor topologies. Subsequently, a Multi-Objective Genetic Algorithm (MOGA) will optimize the asymmetric rotor design, considering mechanical constraints. Finally, the analyses are validated through the testing of a 5 kW spoke-type flux-intensifying PM (SFI-PM) machine equipped with a higher number of FBs in the FD of the q-axis.

II. Analysis Models and Research Method

A. Analysis Models

This study designs a 5 kW spoke-type flux-intensifying PM (SFI-PM) machine with 27 slots and 6 poles, as shown in Fig.

1(a) and (b). This SFI-PM motor, created by incorporating multiple FBs into a conventional spoke-type PM motor, aims to achieve a FI effect, as depicted in Fig. 1(b). The rotor features five FBs: one outer FB (OFB) and four inner FBs (IFBs). The main FB (MFB) is placed on the d-axis to decrease the q-axis inductance (L_q), while the other four FBs are evenly distributed on either side of the q-axis to create the FI effect (where $L_d > L_q$). The specifications and parameters of the SFI-PM motor are listed in Table I. Note that in motor mode, the rotor rotates counterclockwise (CCW), and the PM magnetization direction is perpendicular to the spoke magnet axis (q-axis).

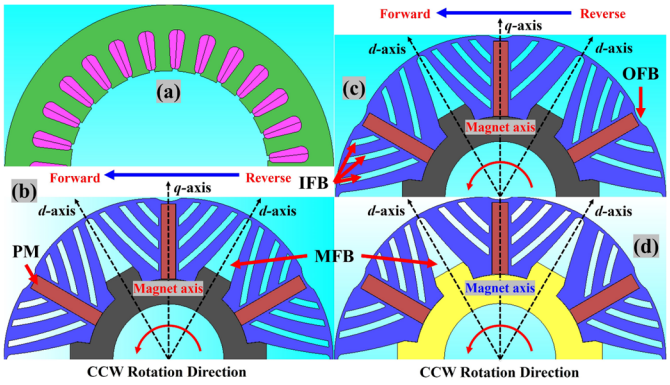

Fig. 1. 5kW SFI-PM motors with different rotor topologies. (a) Stator, (b) symmetric rotor, (c) asymmetric rotor with a higher number of FBs in the RD of q-axis, (d) asymmetric rotor with a higher number of FBs in the FD of q-axis.

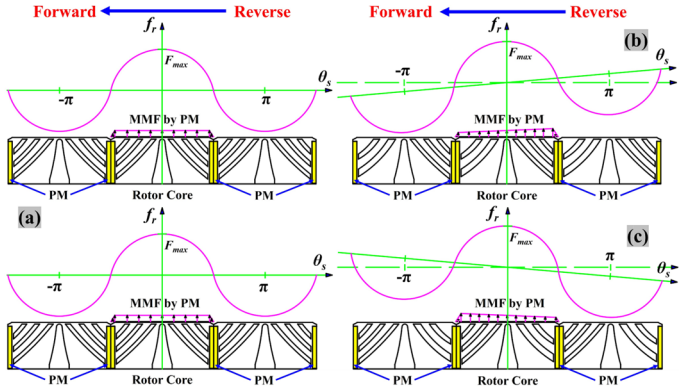

Fig. 2. Magnetic field distribution of rotor MMF by PM. (a) Symmetric rotor, (b) Asymmetric rotor with a higher number of FBs in the RD of q-axis, (c) Asymmetric rotor with a higher number of FBs in the FD of q-axis.

Building upon the symmetric SFI-PM design, the impact of FB positioning to create an asymmetric rotor core is evaluated in two scenarios:

- One of the three IFBs in the RD of the spoke magnet axis (q-axis) along the rotor's rotation is removed, and the other two IFBs are adjusted, as shown in Fig. 1(c).
- Similarly, one of the three IFBs in the FD of the spoke magnet axis (q-axis) along the rotor's rotation is eliminated, with the remaining two IFBs adjusted, as depicted in Fig. 1(d).

The impact of these asymmetric designs is then examined and compared with the symmetrical SFI-PM rotor configuration (Fig. 1(b)), including cogging torque, torque ripple, air gap flux density, and output torque in both the RD and FD of the spoke magnet axis (q-axis).

TABLE I
THE SPECIFICATIONS AND PARAMETERS OF SFI-PM MOTORS

Item	Unit (Value)
Stator Outer/Inner Diameters	160 mm/90.8 mm
Rotor Outer Diameter	90 mm
Stack Length	40 mm
Air gap length	0.4 mm
Peak torque	23 Nm
Maximum/Base speeds	7000 rpm/2000 rpm
Peak power	5 kW
Stator/Rotor materials	35CS250
PM material	N38SH
Input voltage	75 V

B. The MMF of Rotor Comparison

The rotor magnetomotive force (MMF) in the SFI-PM motor is generated by PMs. In a symmetric PM rotor, the assumption is of a uniform air gap and parallel magnetization, resulting in a sinusoidal magnetic field across the air gap, as depicted in Fig. 2. Thus, the rotor MMF is expressed as follows [13]:

$$F_r = F_{max}\, cos(\omega t - \theta_s) \quad (1)$$

$$F_{max} = B_{max}\, \alpha_i g/\mu_0 \quad (2)$$

where B_{max} is the peak flux density produced by the PM in the air gap, ω is the stator's angular frequency, θ_s is the angle between the rotor pole axis and the phase A winding axis around the air gap circumference, α_i is the polar arc coefficient, μ_0 represents the vacuum permeability, and g is the equivalent air gap length.

In a symmetric rotor, PM-generated MMF is evenly distributed. However, in an asymmetric rotor, the rotor core area varies with the number of FBs placed. As the distance between the rotor diameter and PM decreases, permeability and magnetic reluctance increase, leading to asymmetrical MMF [14]. Thus, the MMF generated by PMs in the asymmetric rotor, with a higher number of FBs placed in the FD of the q-axis, can be expressed as follows:

$$F_r^+ = B_{max}\, \alpha_i g/\mu_0 cos(\omega t - \theta_s) \quad (3)$$

The MMF generated by the PMs in the asymmetric rotor, with a higher number of FBs positioned in the RD of the q-axis, can be expressed as follows:

$$F_r^- = -B_{max}\, \alpha_i g/\mu_0 cos(\omega t - \theta_s) \quad (4)$$

III. INFLUENCES OF PLACING FBS IN ASYMMETRIC ROTOR

The influences of placing FBs in an asymmetric rotor on flux density and air gap flux density under no-load conditions are illustrated in Fig. 3. In a symmetric rotor, the flux density remains balanced across the IFB iron segments on both sides of the spoke magnet axis (q-axis). However, in asymmetric rotors, the flux distribution diminishes, varying with the placement of a higher number of FBs on either the RD or FD of the q-axis, as depicted in Fig. 3(a). Consequently, the air gap flux density in the asymmetric rotor slightly increases compared to the symmetric rotor, depending on the FB placement in the RD or FD, as shown in Fig. 3(b).

Fig. 4 compares cogging torque between symmetric and asymmetric rotor configurations. Clearly, placing a higher number of FBs in either the RD or FD of the spoke magnet axis (q-axis) markedly reduces cogging torque. This underscores the

efficacy of asymmetric rotor designs in not only minimizing cogging torque but also reducing torque ripples, noise, and vibration in electric machines.

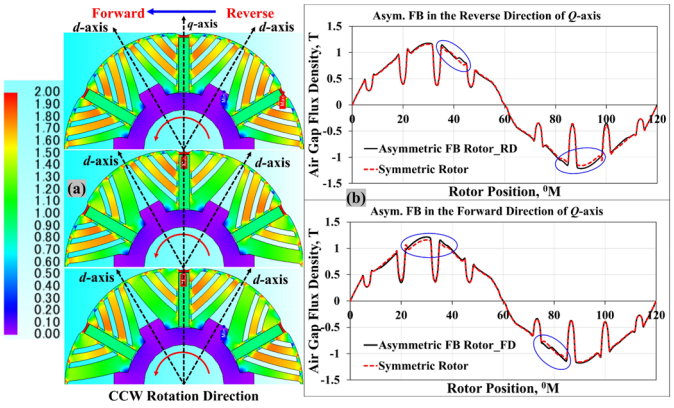

Fig. 3. The comparison of flux density distribution and air gap flux density between symmetric and asymmetric rotors. (a) Flux density distribution, (b) Air gap flux density.

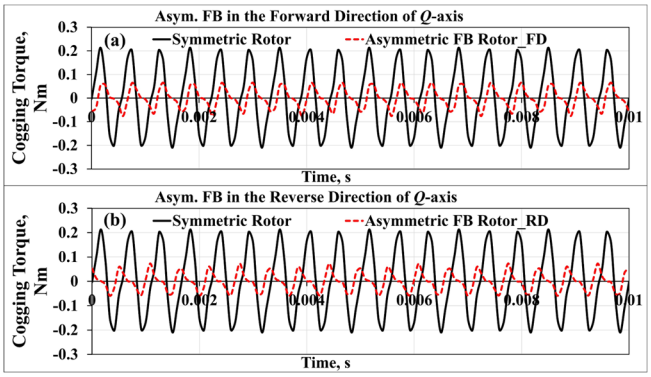

Fig. 4. (a) Cogging torque comparison between symmetric and asymmetric rotors with the higher number of FBs in the forward direction, (b) Cogging torque comparison between symmetric and asymmetric rotors with the higher number of FBs in the reverse direction.

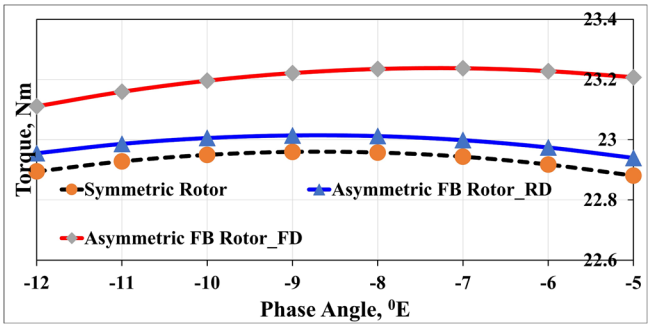

Fig. 5. The output torque comparison between symmetric and asymmetric rotors in the current phase advance angles.

Fig. 5 compares output torque between symmetric and asymmetric rotors under peak operational conditions with current phase advance. Placing a higher number of FBs in the FD of the spoke magnet axis (q-axis) notably enhances output torque in the SFI-PM motor (red line), peaking at approximately 23.3 Nm at a phase advance of -7⁰E. Conversely, maintaining nearly 23 Nm output torque, placing FBs in the RD of the q-axis shows less improvement compared to the symmetric rotor design. However, it results in increased torque ripple (from 19.8% to 21.2%), as shown in Fig. 6(a). In contrast, positioning FBs in the FD of the q-axis decreases torque ripple significantly (from 19.8% to 15.6%), as illustrated in Fig. 6(b). Therefore, placing FBs in the FD of the spoke magnet axis (q-axis) leads to substantial reductions in cogging torque and torque ripple while enhancing output torque.

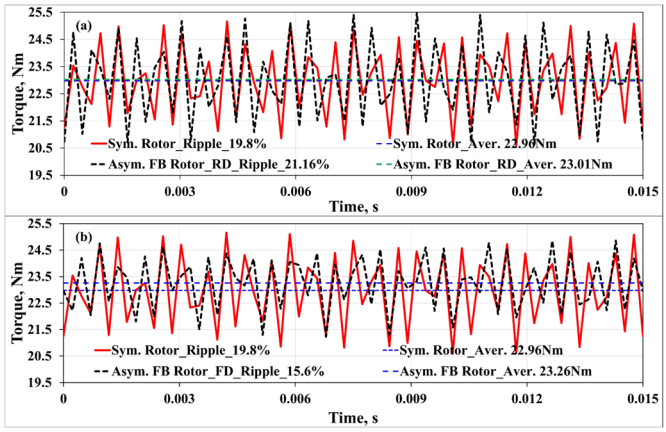

Fig. 6. The output torque comparison between symmetric and asymmetric rotors at peak excitation current.

IV. Design Optimization for an Asymmetric Rotor

Based on the previous analysis, placing more FBs in the FD of the spoke magnet axis (q-axis) provides notable benefits: reduced cogging torque and torque ripple (from 19.8% to 15.6%) and increased output torque (from 22.96 Nm to 23.3 Nm). However, integrating multiple FBs in the rotor still poses challenges, especially in mitigating torque ripples and ensuring mechanical robustness at high speeds. To address these issues, the study employs the Multi-Objective Genetic Algorithm (MOGA) to optimize the asymmetric rotor design with more FBs in the FD, considering mechanical constraints to further enhance motor performance.

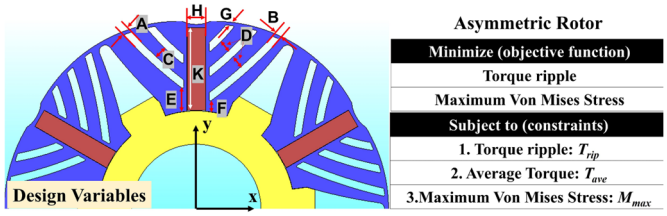

Fig. 7. Design variables and constraints of the rotor for optimization.

The SFI-IPM motor targets electric scooter applications, aiming for torque ripple below 10% to minimize electromagnetic noise and vibrations, with a safety factor of mechanical strength exceeding 2.5. Fig. 7 outlines the rotor design parameters and constraints to achieve these goals. Design variables' maximum and minimum ranges, detailed in Table II, are determined via the design of experiment (DOE) method. The MOGA model uses objective functions and constraints to pinpoint the optimal design point, expressed as follows:

$$\min F(x) = y_1(x) \quad (5)$$

$$\min F(x) = y_2(x) \quad (6)$$

$$\max F(x) = y_3(x) \quad (7)$$

Subject to $G_1(x) = y_1(x) \le T_{rip}$ (8)

$$G_2(x) = y_2(x) \le M_{max} \quad (9)$$

$$G_3(x) = y_3(x) \ge T_{ave} \quad (10)$$

where x is the vector of the design variables, F is the objective function, G is the constraint conditions, y_1 is the torque ripple of the asymmetric rotor, y_2 is the average torque of the asymmetric rotor, and y_3 is the maximum Von Mises Stress of the asymmetric rotor.

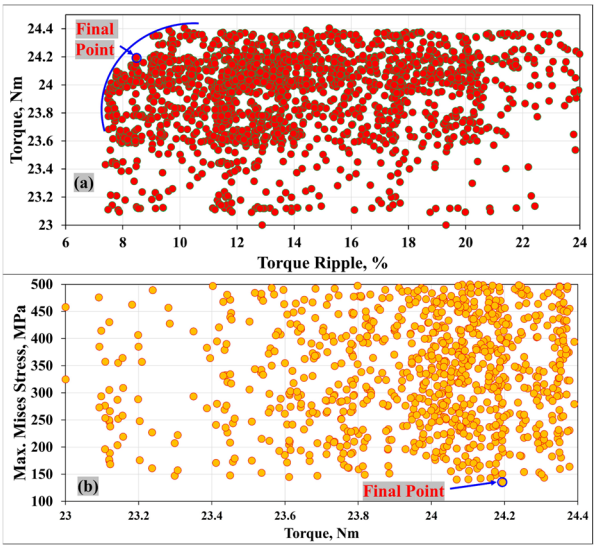

Fig. 8. The multi-objective optimization results. (a) Torque versus torque ripple, (b) Torque versus maximum Von Mises stress.

For the design optimization process, rotor design parameters' objectives and constraints are defined within the Finite Element Analysis (FEA) package, JMAG. The MOGA is selected as the optimization engine with tailored settings: 100 generations and a population size of 100. Over 1000 optimization cases are computed and visualized in Fig. 8.

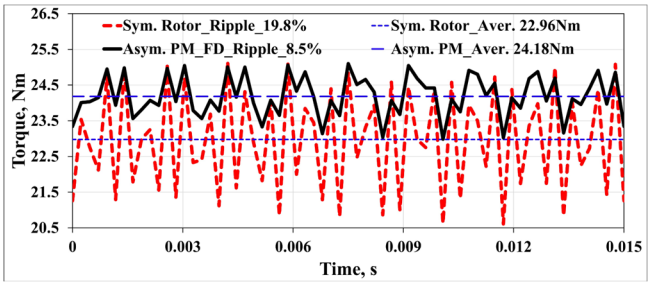

Fig. 9. The output torque comparison before and after optimization.

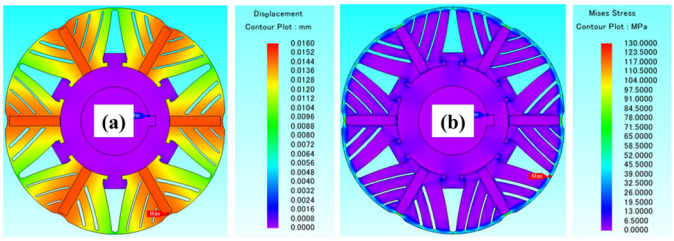

Fig. 10. Displacement and the Von Mises Stress distributions of asymmetric SFI-PM motor at 7000 rpm.

After completing the multi-objective optimization using a genetic algorithm, the results in Fig. 8 illustrate both the Pareto front and the generated partial solutions. Based on these findings, dimensions were carefully selected and presented in Table III after a comprehensive evaluation. Fig. 9 shows the output torque results of the initial and optimized models, indicating a significant improvement from 22.96 Nm to 24.2 Nm, along with a reduction in torque ripple from 15.6% to 8.5%. Additionally, the asymmetric SFI-PM motor exhibits a maximum displacement of 0.016 mm and centrifugal force of 135 MPa, ensuring mechanical stability with a safety factor exceeding 2.5, as shown in Fig. 10.

TABLE II
THE RANGE OF OPTIMIZED PARAMETERS OF SFI-PM MOTORS

Parameters	Min (mm)	Max (mm)
A	0.2	2
B	0.2	2
C	3	6
D	3	6
E	5	7
F	3	5
G	0.8	1.5
H	4	5.5
K	20	25

TABLE III
THE DESIGN PARAMETERS COMPARISON

Parameters	Before Optimization	After Optimization
A (mm)	1.2	1.7
B (mm)	1.2	0.9
C (mm)	3.5	3.6
D (mm)	3.6	4.1
E (mm)	5.8	5.7
F (mm)	3.6	3.2
G (mm)	1	1.1
H (mm)	5	4.6
K (mm)	22	20.5

V. EXPERIMENTAL STUDY

To validate these findings, a prototype of the 5 kW asymmetric SFI-PM machine was manufactured, and experimental studies were conducted. Fig. 11 shows the rotor prototype of the 5 kW asymmetric SFI-PM motor with additional FBs in the FD of the spoke magnet axis. During the no-load testing phase, magnetic flux density distribution on the rotor core was measured. Experimental results from the no-load testing of magnetic flux density for the 5 kW asymmetric SFI-PM are presented in Fig. 12. The simulation indicates a maximum flux density distribution of 0.19 T, evenly spread across the six poles, as depicted in Fig. 12(a). In contrast, experimental results show a slightly lower and uneven distribution among the pole pairs, likely due to manufacturing tolerances in the prototype. However, this variance falls within an acceptable range, affirming the alignment between experimental and simulation outcomes.

Fig. 13(a) compares the back EMF of the asymmetric SFI-PM motor in simulation and experimentation at 2000 rpm. The oscilloscope-recorded waveform closely matches the simulation, showing a smooth sinusoidal curve indicative of anticipated torque stability under load conditions. Fig. 13(b) also proves that there is consistency between simulation and experimental back EMF at various speeds, confirming the accuracy of the analysis.

Due to the unavailability of a suitable driver and test bench limitations, the motor was tested under direct current instead of maximum conditions. Fig. 13 compares simulation results with actual experimental data at 60 A. In Fig. 14(a), variations in output torque with respect to the current phase advance angle are shown, reaching rated torque values of 13.5 Nm in simulation and 12 Nm in experimentation at a negative current phase advance angle of -5°E. Fig. 14(b) compares the output torque waveform at a rated current of 60 A, revealing a torque ripple of 8.5% in the simulation and 8.8% in the experiment. It's important to note that using direct current affects the motor's L_d and L_q values, limiting its reluctance torque capabilities and resulting in slightly reduced output torque during experimental testing.

Despite the limitations in load testing, these experimental results sufficiently validate the accuracy of the analyses.

Fig. 11. The rotor prototype of a 5 kW asymmetric SFI-PM motor with a higher number of FBs in the FD of the spoke magnet axis and no-load magnetic flux density distribution testing on the rotor core.

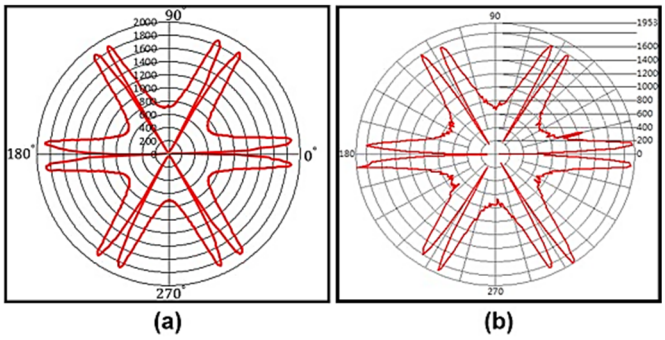

Fig. 12. Magnetic flux density distribution on the rotor core. (a) Simulation, (b) Measurement.

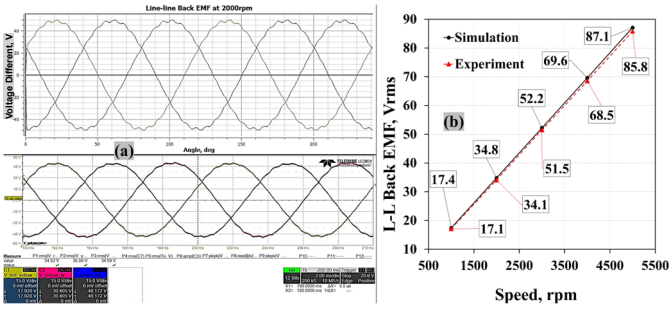

Fig. 13. (a) Simulation and measurement comparison of back EMF at 2000 rpm, (b) Simulation and measurement comparison of back EM with different speeds.

VI. Conclusion

This study analyzed the strategic placement of flux barriers in the asymmetric rotor to enhance SFI-PM motor performance. The effects of positioning a higher number of flux barriers in the forward or reverse directions of the spoke magnet axis (*q*-axis), aligning with the rotation direction of the rotor, on cogging torque, output torque, and torque ripple were thoroughly investigated and compared to a symmetrical SFI-PM motor. Results show that placing more flux barriers in the forward direction of the spoke magnet axis significantly reduces cogging torque and torque ripple while improving output torque. To validate these findings, a 5 kW asymmetric SFI-PM machine with flux barriers in the forward direction was fabricated and tested. The experimental results closely matched the simulations, confirming the analysis.

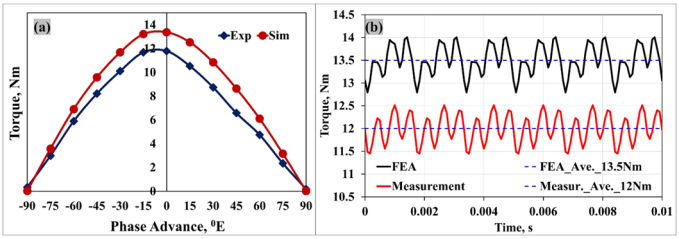

Fig. 14. The output torque comparison between simulation and experiment. (a) Torque versus current phase advance, (b) Torque waveform at 60A.

References

[1] X. Zhu et al., "Comparative Design and Analysis of New Type of Flux-Intensifying Interior Permanent Magnet Motors with Different Q-Axis Rotor Flux Barriers," *IEEE Trans. Energy. Conver.,* vol. 33, no. 4, pp. 2260-2269, 2018.

[2] T. Wang et al., "Investigation on Torque Characteristic and PM Operation Point of Flux-Intensifying PM Motor Considering Low-Speed Operation," *IEEE Trans. Magn.,* vol. 57, no. 2, pp. 1-5, 2021.

[3] T. A. Huynh et al., "Influence of Flux Barriers and Permanent Magnet Arrangements on Performance of High-Speed Flux-Intensifying IPM Motor," *IEEE Trans. Magn.,* vol. 59, no. 11, pp. 1-5, 2023.

[4] M. H. A. Prins, "*Design of a Field-Intensified Interior Permanent Magnet Synchronous Machine for Electric Vehicle Application*," Master Thesis of Science in Electrical and Electronic Engineering at the University of Stellenbosch.

[5] M. Kashif, B. Singh, "Design optimization with improved torque performance of a new flux intensifying PMSM using multilayer barriers for solar water pumps," *Engineering Science and Technology, an International Journal*, vol. 36, 101134, 2022.

[6] M. Kashif, B. Singh, "Improvement of torque and permanent magnet operating flux density in a novel flux-intensifying spoke PMSM based on peripheral and internal barriers," *Sådhanå*, vol. 47, no. 42, 2022.

[7] Y. Xiao et al., "A Novel Spoke-Type Asymmetric Rotor Interior Permanent Magnet Machine," *IEEE Trans. Ind. Appl.*, vol. 57, no. 5, September/October 2021.

[8] Y. Xiao et al., "A Novel Asymmetric Interior Permanent Magnet Machine for Electric Vehicles," *IEEE Trans. Energy. Conver.,* Vol. 36, No. 3, September 2021.

[9] Y. Xiao et al., "A Novel Asymmetric Rotor Interior Permanent Magnet Machine with Hybrid-Layer Permanent Magnets," *IEEE Trans. Ind. Appl.*, vol. 57, no. 6, November/December 2021.

[10] T. Takahashi et al., "Reluctance Torque and Output Improvement of Concentrated Winding IPMSM With Asymmetric Slit," *IEEE Trans. Ind. Appl.*, vol. 59, no. 6, November/December 2023.

[11] H. Yang et al., "A Novel Asymmetric-Magnetic-Pole Interior PM Machine with Magnet-Axis-Shifting Effect," *IEEE Trans. Ind. Appl.*, vol. 57, no. 6, November/December 2021.

[12] Y. Li et al., "A Novel Magnet-Axis-Shifted Hybrid Permanent Magnet Machine for Electric Vehicle Applications," *Energies*, vol. 12, 641, 2019.

[13] J. Zhang et al., "Influence of Introducing the Rotor MMF Harmonic on Torque Performance of Spoke Type Permanent Magnet Motor With FSCW," *IEEE Access*, vol. 8, 2020.

[14] J.-C. Park et al., "Design Optimization Using Asymmetric Rotor in IPMSM for Torque Ripple Reduction Considering Forward and Reverse Directions," *IEEE Trans. Magn.,* vol. 59, no. 11, pp. 1-5, 2023.